STARS TRAPPED AT THE BAR RESONANCE

LIU REPORT

by

Adrian SZPILFIDEL

Under the guidance of

Paola Di Matteo

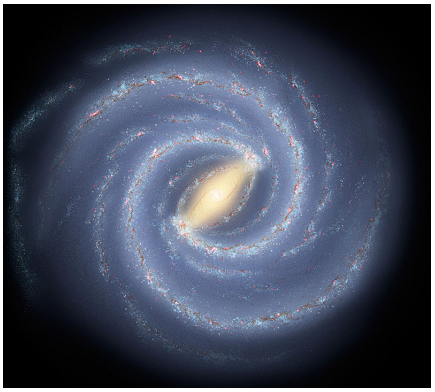

Galaxies, Étoiles, Physique et Instrumentation (GEPI)

Observatoire de Paris, Paris Sciences et Lettres

From September 10th 2024 to December 11th 2024

Observatoire de Paris | PSL

Acknowledgements

I express my gratitude to Paola Di Matteo for supervising me during my internship and for giving me the opportunity to explore galactic physics. I also thank Salvatore Ferrone for taking the time to introduce me to numerical simulations and for sharing his work on the code with me. Thank you to Tristan Boin for helping me during this internship.

Lastly, a big thanks to the entire GEPI team for making me feel welcome.

Abstract

A large fraction of disk galaxies have a bar. It is a massive rectangular structure composed of stars, located in the inner region. The bar rotates at a certain speed and creates a asymmetric potential in the galaxy. Its features, such as mass, rotation pattern speed, and shape, determine the fate of stars in the disk. Indeed, the bar creates resonances; stars at resonance form closed orbits in the bar reference frame, seeing the bar periodically at a certain frequency. The real impact of the bar's features is still a subject of discussion, and it is challenging to properly determine the exact characteristics of a bar.

The objective of this lab insertion unit (LIU) is to study the effect of the bar by looking at the stars trapped at the resonance. To do so, we used numerical simulations of disk galaxies. The challenge of this LIU is to delve into large codes that are already written but to use them in a context for which they were not initially designed.

We have to use different codes independently to generate the initial conditions and compute the integration. Afterwards, we calculate the orbital frequencies to illustrate the resonances and select particles trapped at resonance to study their movement in the galaxy.

The simulation shows that the bar has a strong effect on the particles in the disk; its mass and rotation speed determine the parameters. The bar is clearly visible through the set of particles. Computing the Fast Fourier Transform (FFT) on the orbits shows resonances at corotation, inner Lindblad resonance, and outer Lindblad resonance.

Contents

Introduction

Galaxies can be classified into different types: elliptical and disk galaxies. More than half of the local universe is filled with large disk galaxies, and they are the most efficient at converting gas into stars. Galaxies are composed of a dark matter halo, stars, gas, and dust. The inner part of the galaxy (within a radius of 1 kpc) is dominated by the bulge. Farther away (from 1 kpc to 10 kpc), the disk dominates. One way to represent the galactic disk is to separate it into two disks: the thin disk and the thick disk. For the Milky Way, the thick disk is 2 kpc long and 0.8 kpc high, while the thin disk is 5 kpc long and 0.25 kpc high. Disk galaxies may contain a bar at the center, which is part of the bulge, as it is well explained in Combes 2023. This rectangular feature is a denser area in the galaxy, characterized by its mass, pattern velocity, etc. The key point of a barred galaxy is that it has orbital resonances in the galactic disk. The most important resonance is the corotation, defined by the stars that rotate at the same angular velocity as the bar. The mean position of these stars is fixed as long as the bar's features do not evolve.

Low-metallicity stars have been observed at the edges of galaxies; these stars should normally be located in the inner region of the disk, where there is more star formation. A possible reason for their presence in the outer areas could be radial migration, possibly caused by an evolution of the bar's properties.

The main objective of this work is to analyze the impact of the bar on orbits in the disks. To do so, we have used test-particle simulations.

The work accomplished during this LIU can be separated in two parts. The first one was about learning the basics of galactic dynamics by reading articles, courses (e.g Bovy n.d.) and integrating orbits in symmetric potentials to get used to the tstrippy code. In a second part, we studied asymmetric potentials, such the Milky Way, that contains a bar at the center. We use a code originally developed by Paola Di Matteo, and then updated by S. Ferrone in Ferrone et al. 2023. A second version of this code, significantly restructured, has been developed by S. Ferrone, during his PhD. For my LIU I have been using this second, still unpublished, version of the code and I have tested and used it in a different context (dynamics of disc stars in barred galaxies) from which it was originally developed (dynamics of stellar streams in galactic halos). We input the form of the galactic potential, corresponding to the sum of the potential of the different components. This potential depends on the galaxy's features. When adding the bar potential, the total potential becomes asymmetric and evolves over time. The particles only interact with the galactic potential; there is no interaction between them. This is different from direct N-body simulations, where all particles experience the gravitational attraction of all the other particles in the system. Once the galactic parameters defined, we generate positions and velocities of (thin and thick) disk particles at equilibrium in this potential, by making use of the publicly available AGAMA library (Vasiliev 2018). Afterward, we add to the axisymmetric potential the bar component, and integrate the orbits of these particles in this asymmetric potential. Finally, we determine the stars at resonance and observe how they behave on a large timescale.

The report is structured as follows : firstly, we explain the physical model of galaxies and orbits in section 1. In section 2, we detail the method used to process the simulation. Then, in section 3, we discuss the results obtained and finally, we conclude with some discussions and conclusions about the impact of the bar's feature evolution on stars at resonance.

1 Framework of galactic dynamics

The potentials for the galaxy simulation conducted in this work have been developed in Pouliasis et al. 2017. They consist of a sum of different potentials for each component of the galaxy: halo, bulge, thin disk, and thick disk.

1.1 Axis-symmetric potential

1.1.1 Plummer potential

Developed in Plummer 1911, it is a spherically symmetric potential that only depends on the spherical radius $r = \sqrt{x^2 + y^2 + z^2}$. This spherically symmetric potential is often used in galactic dynamics, to describe the mass distribution of bulges, as well as cored dark matter halos or stellar systems as globular clusters. It is given by:

$$\Phi_{plummer}(r) = -\frac{GM}{\sqrt{r^2 + b^2}} \tag{1}$$

Where b is a parameter of the distribution. Using the Poisson equation $\Delta\Phi = 4\pi\rho G$, one can find the associated mass distribution ρ:

$$\rho_{plummer}(r) = \frac{3b^2 M}{4\pi(r^2 + b^2)^{5/2}} \tag{2}$$

An example of an orbit integration in a plummer potential is reported in Appendix A.

1.1.2 Disk potential

For the disk, the potential is a Miyamoto-Nagai type (Miyamoto et al. 1975). This is an axis-symmetric distribution that depends on $R = \sqrt{x^2 + y^2}$, the radius in the plane (x, y), and z, the height. We have used this density profile because it is one the most widely used disk potentials, because of its simplicity.

$$\Phi_{disk}(R, z) = -\frac{GM_{disk}}{\sqrt{R^2 + (a + \sqrt{z^2 + b^2})^2}} \tag{3}$$

The associated mass density distribution is:

$$\rho_{disk}(R, z) = \frac{b^2 M_{disk}}{4\pi} \frac{aR^2 + (a + 3\sqrt{z^2 + b^2})(a + \sqrt{z^2 + b^2})^2}{(R^2 + (a + \sqrt{z^2 + b^2})^2)^{5/2}(z^2 + b^2)^{3/2}} \tag{4}$$

The parameters a and b correspond respectively to the characteristic length and height. Note that using $a = 0$ in (4) is equivalent to the Plummer mass density distribution (2).

1.2 Barred galaxy

Disk galaxies like our own are known to possess a stellar bar in their central regions. Bars are made of stars with different orbits, which are collected in such a way that the bar rotates as a rigid body around the galactic center. The angular velocity at which a bar rotates in a disk galaxy is known as "pattern speed", written $\Omega_{\rm p}$. Orbits are unclosed in the galactic potential because the potential is not Keplerian. There are orbital resonances in the galactic disk, meaning that some stars are trapped in a potential well and their orbits are closed in the reference frame of the bar.

1.2.1 Bar potential

As a model for the bar, we have used the triaxial model presented by Long et al. 1992. This model can be seen as "a triaxial extension" of the Miyamoto-Nagai disk.

$$\Phi_{bar}(R, x) = \frac{GM_{bar}}{2a} \ln\left(\frac{x - a + \sqrt{(a - x)^2 + y^2 + (b + \sqrt{c^2 + z^2})^2}}{x + a + \sqrt{(a + x)^2 + y^2 + (b + \sqrt{c^2 + z^2})^2}}\right) \tag{5}$$

1.2.2 Orbital resonances

A star experiences three different oscillations in a galaxy: radial, azimuthal, and vertical. Each of these oscillations is described by a set of frequency: respectively κ, Ω, and ν. The orbital resonances are the most important feature induced by the presence of the bar. A particle trapped at resonance with the bar feels strong effects from it. In the bar reference frame, in which the bar is fixed, its orbit is closed, meaning that the gravitational potential felt by the particle oscillates periodically, this is a resonance. There are three main resonances: Corotation (CR), Outer Lindblad Resonance (OLR), and Inner Lindblad Resonance (ILR). The shape of these orbits is reproduced in Figure 1, figure from Combes 2023. Stars at corotation resonance rotate at the same speed as the pattern speed: $\Omega = \Omega_{\rm p}$. In the bar frame, the clockwise rotating frame, their orbit appears as a point or small ellipse around a mean radius (see center plot in Figure 1). Beyond the mean radius, they orbit counterclockwise, and below the mean radius, they move clockwise. This is because when they are farther than the corotation radius, their angular velocity $\Omega < \Omega_{\rm p}$, and vice versa. At the inner Lindblad resonance (ILR): $\Omega - \Omega_{\rm p} = \kappa/2$. This means that in the rotating bar reference frame, the azimuthal frequency is half the epicyclic frequency (see left plot in Figure 1). For one rotation, the star completes two radial oscillations. In the inner region, the stars rotate faster than the bar, and the orbit is clockwise. At the outer Lindblad resonance (OLR): $\Omega - \Omega_{\rm p} = -\kappa/2$. As with the inner Lindblad resonance, the stars complete two radial oscillations during one revolution in the bar reference frame. However, their trajectories are counterclockwise because they rotate slower than the bar.

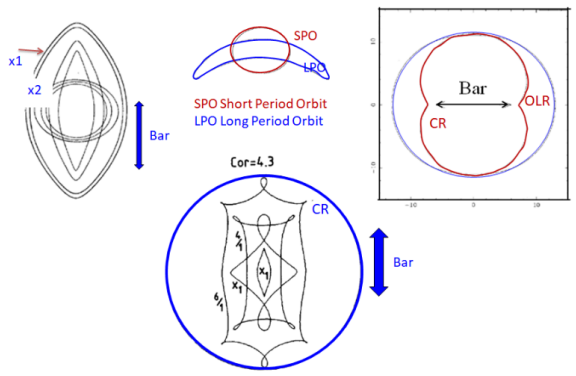

Figure 1: Orbits at resonances, figure reproduced from Combes 2023, initially reproduced from Contopoulos et al. 1980.

2 Method

The aim of this LIU has been to use the code tstrippy to simulate the evolution of disc particles in a barred potential. The general method is to process particle-test simulations in order to calculate the orbits of particles in a galactic potential. The potential results from a sum over the analytical potential of the galaxy components (disks, halo and bar). The particles are meant to test the movement within the galaxy, they only interact with the potential. This is very different from N-body simulations where there is no analytical potential but the potential created by each particle. Such simulations can also show orbital resonances (e.g Ceverino et al. 2007). The computation of this method can be separated in several steps : 1. Choose the galactic parameters; 2. Generate initial conditions; 3. Fix the bar's parameters; 4. Compute the orbital frequencies; 5. Select orbits at resonance.

2.1 Models of disks and halo

We fix the parameters of the galaxy using the Milky Way parameters. Initially, there are three components in the galaxy simulation : the halo, the thin and thick disks. The parameter values are fixed with according to the Milky Way parameters. The important parameters are the mass, the scale length a and the scale height b.

	Mass $[M_\odot]$	a [kpc]	b [kpc]
Halo	$2.088e+11$	14	–
Thin disk	$3.712e+10$	4.8	0.25
Thick disk	$3.944e+10$	2	0.8

Table 1: Galactic parameters

2.2 Generate initial conditions

The code takes as an input the initial conditions of the galaxy population. We need to generate initial conditions for a large number of particles. These initial conditions cannot be completely random, because the system would be unstable. When starting the integration to properly see the bar effect, the galaxy has to be in an equilibrium state. In order to generate a large number of particles in equilibrium with the galactic potential (without bar), we use the library AGAMA (see Vasiliev 2018). We fix the components of the galaxy and their features, i.e., mass, radius, type of potential, etc. Then we create the required potential. For the disks, we use the Miyamoto-Nagai potential. For the dark matter halo, we use the model A&S presented in Ferrone et al. 2023. The potential used in AGAMA for the halo is not exactly the same, because it is a Plummer potential (1), but it is quite similar for low radii around 10 kpc. Afterward, we generate the model and a population of disk particles.

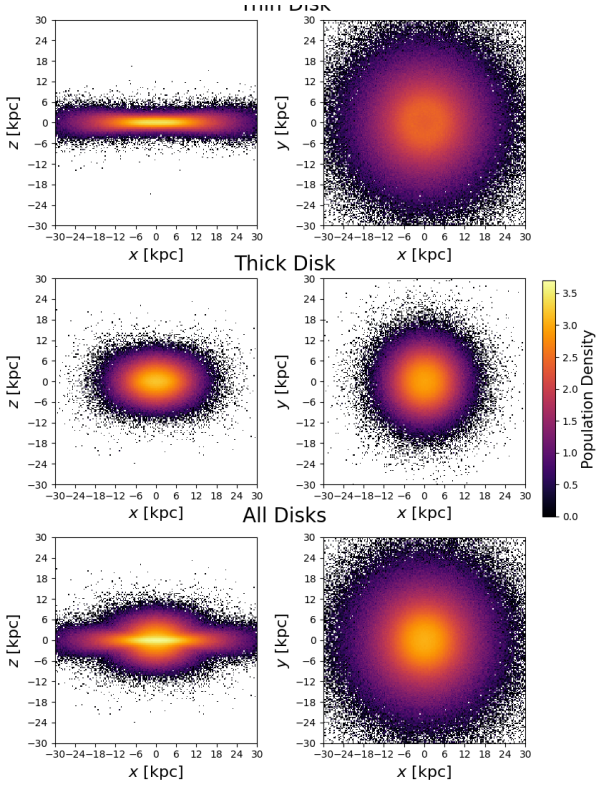

Figure 2: Initial population in the disks with 2×10^6 particles. Left column is a transverse view, right column is a view from above. The first row shows the thin disk particles, the second row shows the thick disk particles and the last row is both disks gathered. The units are in kiloparsec [kpc]

We can see in right column plots of Figure 2, the population density view in the plane (x, y), that the distribution only depends on the radius, it is almost axis-symmetric.

In order to verify the model is actually stable, we run a simulation with these initial conditions, without any bar, with the exact same potential used to generate the model. To avoid long computation, we

ran these test with 5k particles in each disk. By plotting galactic density map at initial time and after several billion years, we ensure that the disks have kept their initial properties, in terms of size and mass distribution. If they have not, it means that the system was not at equilibrium. As we can see in Figure 3 and Figure 4, the results are satisfying. There are no changes in the general shapes of the disks and in the profiles.

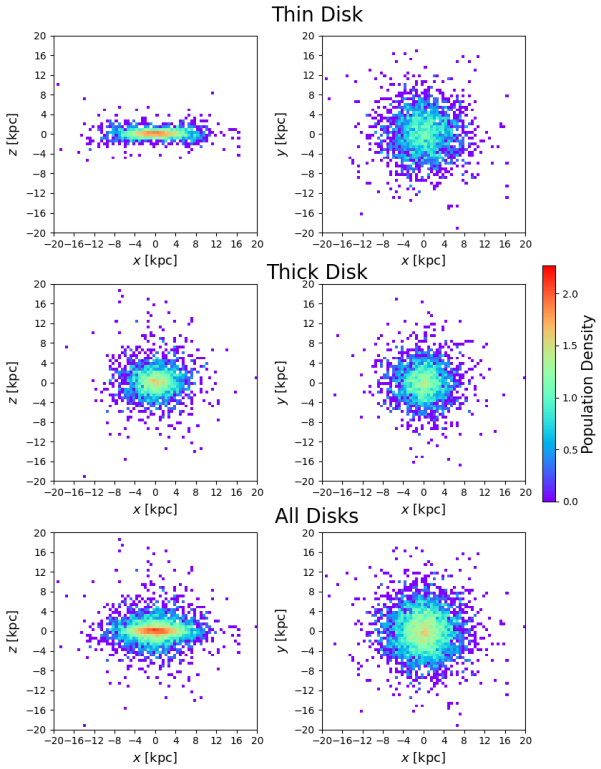

Figure 3: Final density map after integration over 5 Gyr, for 10×10^3 particles in the disks.

We can also verify the mass density profile at the initial time and final time (see Figure 4). To do this, for each value of the radius in the galactic plan $R = \sqrt{x^2 + y^2}$, we count the number of particles contained in the ring of surface $\sigma = \pi(R_{i+1} - R_i)^2$. We can either multiply by the mass to have the mass density profile or just use the number density profile. We see in Figure 4 that the thick disk dominates at low radius and then, after 4 kpc the thin disk dominates. The shape of the disks is stable during the integration after 5 Gyr.

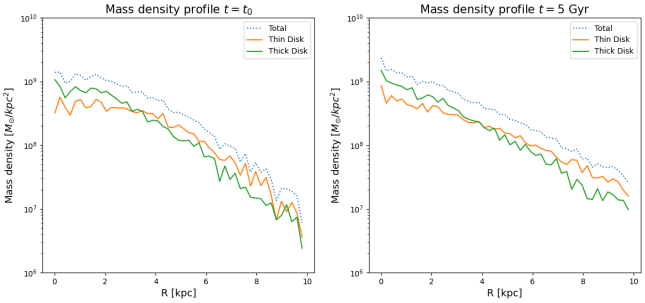

Figure 4: Mass density profile stability check of thin disk and thick disk

The vertical number density profile is also interesting, it highlight the difference between the thin disk and the thick disk. And it is useful to check the stability condition on the disks shape. To compute it, we count the number of particle contained in the segment $[z, z + dz]$ for a given radius interval, then the number density is the number of particles divided by the length dz. This analysis is reported in

Figure 5. At low z, the thin disk dominates the number density, when z increases the number density of the thin disk fastly decreases and the thick disk dominates. This is coherent with the parameters that we used, in Table 1.

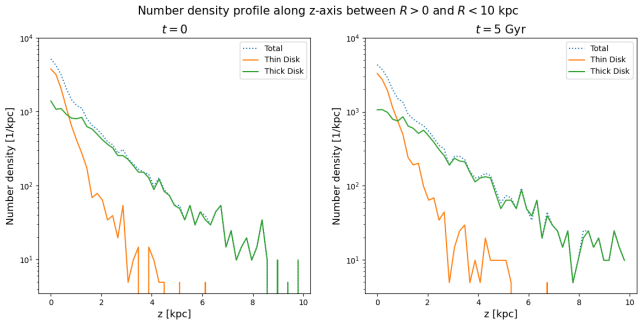

Figure 5: Vertical number density profile stability of thin disk and thick disk

2.3 Model of the bar

The next step is to add the bar in the galactic potential. To simulate the bar, we use we use the bar triaxial potential described in Long et al. 1992, see previous relation (5). The relevant parameters for the bar are the mass, the scale length a, the scale width b, the scale height c and the pattern speed Ω_{p}.

	Mass $[M_\odot]$	a [kpc]	b [kpc]	c [kpc]	Ω_{p} [km/s/kpc]
Bar	$2.2968e+10$	4	0.1	0.5	31.05

Table 2: Bar parameters

To determine the bar pattern speed, we need to analyze the angular velocity profile of the particles in the disk, depending on the radius R.

The angular velocity is given by :

$$\omega = \frac{v_t}{R}$$

Where $v_t = \frac{xv_y - yv_x}{R}$ is the tangential velocity in the galacitc plane. We want to restrict the analysis on the thin disk particles because they have less vertical excursion. For each value of the radius, the particles have different angular velocity ω, spread around a mean value. We compute this mean value, by adjusting the length of the bin with the number of particles. We fix the corotation radius at 6 kpc, because this value is similar to the estimated bar corotation radius in the Milky Way disk. We could have chosen an other value, it is arbitrary. Then the bar pattern speed is given by the mean angular velocity at $r = 6\,\text{kpc}$. By doing an interpolation, in Figure 6, with the value of each bin, we find the intersection $\Omega_{\text{p}} = 31.05\,\text{km}\,\text{s}^{-1}\,\text{kpc}^{-1}$.

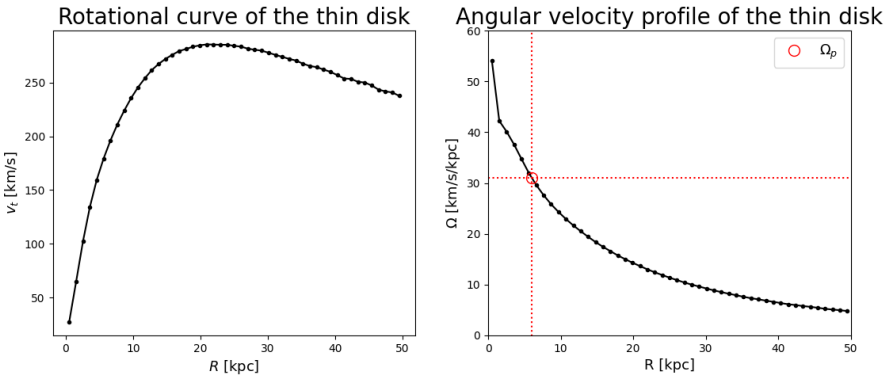

Figure 6: (Left panel) Plot of the rotational curve of the thin disk, each point is the mean value of the tangential velocity of the particles within the bin. (Right panel) Angular velocity, tangential velocity divided by R for each bin.

We can also see in Figure 6 the flatten of the rotational curve, due to the dark matter halo.

3 Results

3.1 Formation of the bar

After running the code during $T = 5$ Gyr, we obtain results of the galaxy evolution. The first thing to look for is the formation of the bar. We can observe the particles accreting along the bar during the simulation, as shown in the density map (see Figure 7). After 125 Myr, the bar shape is stable and does not change.

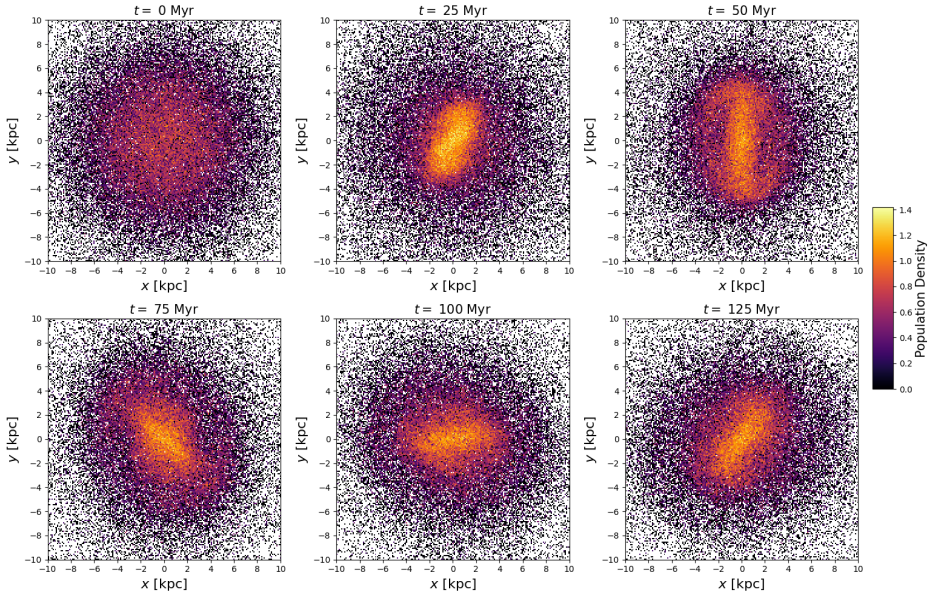

Figure 7: Bar formation during the beginning of the integration up to 125 Myr, with 80k particles. In the bar reference frame. The units are in kiloparsec.

3.2 Bar resonances

To find the particles that are at resonance with the bar we need their orbital frequencies. We have all the positions and velocities of each particle for each time step. For each particle, we want a value for (κ, Ω, ν), the orbital frequencies introduced in 1.2.2. In order to obtain these orbital frequencies, we process Fast Fourier Transform (FFT) on the signal corresponding to the radius in the galactic plane $R(t) = \sqrt{x(t)^2 + y(t)^2}$, the angle $\theta(t)$ between the particle and the x-axis and the vertical positions

$z(t)$. The signal might be composed of several frequencies for a given particle, we keep only the frequency with the highest amplitude.

We observe that the distribution of the particles form peaks around resonances value, we show this the Figure 8 is the number of particles in logarithm scale as a function of $\frac{\Omega-\Omega_p}{\kappa}$. When it is equal to 0, it corresponds to the corotation resonance (CR), 0.5 value corresponds to inner Lindbald Resonance (ILR) and -0.5 to outer Lindbald resonance (OLR), as explained in 1.2.2.

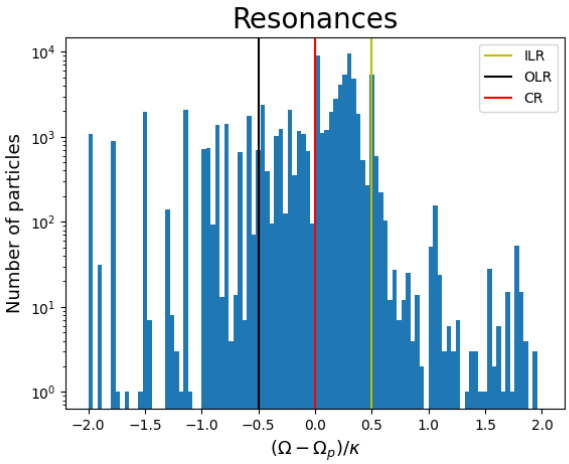

Figure 8: Histogram showing the number of particles with respect to the quantity $\frac{\Omega-\Omega_p}{\kappa}$. The vertical lines represent the three orbital resonances of interest.

Let us look closer to the typical shape of the orbits at resonances.

3.2.1 Corotation Resonance

The Figure 9 shows two orbits of a particle near to corotation. We see that it is consistent with the orbit predicted by the theory, we observe small circles around the mean radius of 5.75-6.75 kpc. The color legend shows that the particle is turning clockwise as predicted. However, the orbit doesn't draw perfect circle because it is not exactly at $\Omega = \Omega_{\mathrm{p}}$ but very close.

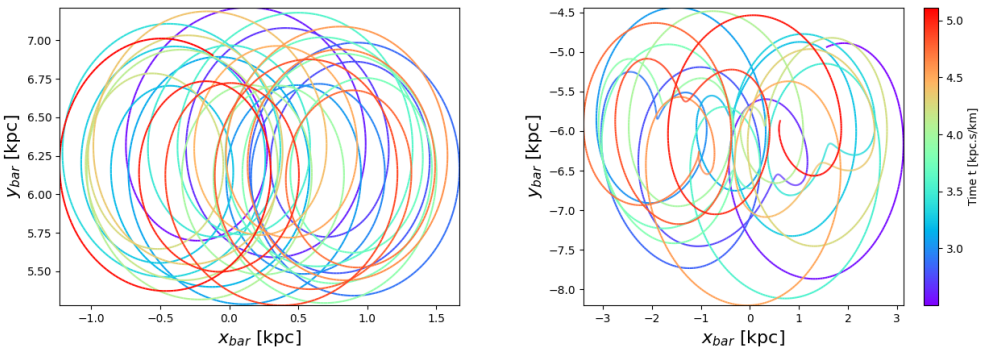

Figure 9: Orbit of a particle near the corotation in the bar reference frame. The left orbit represent a particle located above the bar at Lagrange L5, and the right panel represent a particle located below at Lagrange point L4, in the bar reference frame.

3.2.2 Inner Lindbald resonance

Looking closer at ILR orbits, we find orbits like Figure 10. The orbit is closed and draws circles around the bar, with very small radial excursions. When looking at the color, that highlight the time, we see that the particle is turning clockwise, meaning that it goes faster than the bar pattern speed. This

is exactly what we expected, by definition of the ILR as seen in 1.2.2. We also emphasize that the particle draw ellipses around the bar, the semi-long axis of its orbit is exactly the characteristic length of the bar,$a = 4$kpc set in Table 2.

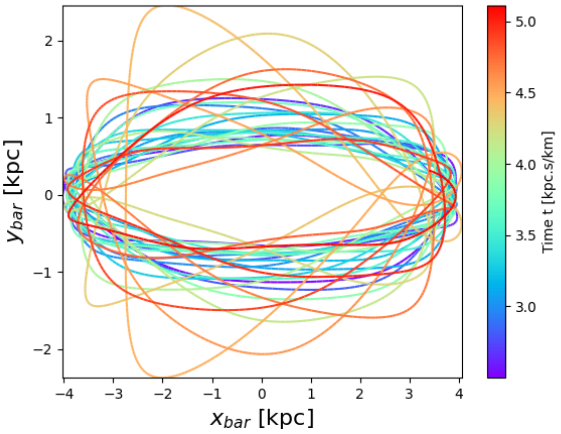

Figure 10: Orbit at ILR in the bar reference frame

3.2.3 Outer Lindbald resonance

Now we are looking at OLR orbits and we find orbits that have shape showed in Figure 11. The orbit is perfectly circular in the bar reference frame, it correspond exactly to what we expected (see right plot in Figure 1). We can observe that the orbit makes larger radial excursions (from -15 kpc to 15 kpc), and counterclockwise this time, because the particle is farther than the corotation radius and turns slower than the bar.

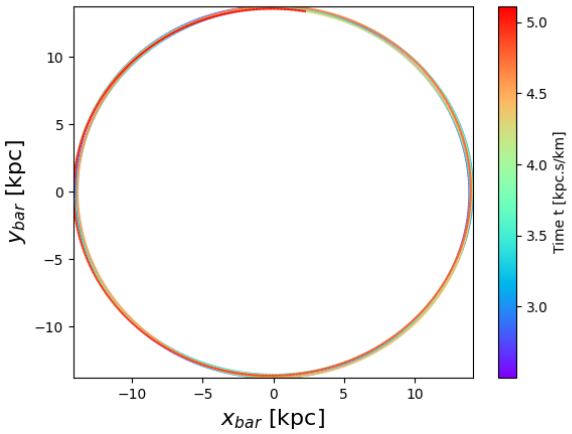

Figure 11: Orbit of a particle at OLR, in the bar reference frame.

Conclusion and discussions

In conclusion, we have observed the effect of the bar on particles in disk galaxies in this work. The bar is a rotating structure located in the inner region of most galaxy disks. Numerical simulations, computed with the leapfrog method, show that the presence of a bar with a specific rotation speed creates a strong influence on stars by creating resonances. After a time integration of 5 Gyr, we observed resonances such as corotation (CR), outer Lindblad resonance (OLR), and inner Lindblad resonance (ILR). The effect of the bar depends on its mass and its rotation velocity. These effects can be probed through particles at resonances. A general orbit in a galactic potential is not closed and

forms a rosette. The orbits of particles trapped at resonance form closed orbits in the bar's reference frame. When a particle is trapped at resonance, it remains under its influence. We saw that fixing a value for the angular speed of the bar determines the corotation radius.

More generally, this work demonstrates an example of gathering different codes that were not built for the same purpose. We ran particle test simulations in a barred galaxy. We used AGAMA to generate initial conditions at equilibrium in the galactic potential composed of a dark matter halo, a thick and thin disks, with a large number of particles. After verifying that the conditions were stable enough, we integrated these particles in a galactic potential to which we added a bar potential. By computing the Fast Fourier transform on the variation of the radius, azimuthal angle, and height of all particles, we highlighted the distribution of resonances in the galaxy. The orbits of these resonances correspond to what is expected.

An improvement can be made in the generation of initial conditions. The fact that the potential for the dark matter halo was a Plummer potential and different from the halo potential used in the integration can have a small effect. Furthermore, we observed a lot of noise in the distribution of the particles as a function of their orbital frequencies. By selecting particles near resonances such as CR, ILR, and OLR, we saw that the selection is polluted with particles that are not at resonance. The origin of this problem needs much more time to be investigated. Finally, an interesting perspective to this work would be to explore the effect of evolving parameters for the bar and observe the effect on stars at resonances.

A Plummer shpere

The force felt by a particle at a distance R from the center in a Plummer potential (1) is equivalent to the force created by a point-mass source at the center of the distribution with a mass equal to the mass enclosed within the radius R. The mass enclosed within a radius r_0 is:

$$M(< r_0) = \int_{V(r_0)} \rho_{plummer}(r)\mathrm{dV} = M_{tot}\left(1 + \frac{b^2}{r_0^2}\right)^{-3/2} \tag{6}$$

Then we can build the tangential velocity required in the initial conditions to obtain a circular orbit. This velocity is:

$$v_\theta = \sqrt{\frac{GM(< r_0)}{r_0}} \tag{7}$$

To get familiar with the tstrippy code, I first tested basic orbit integrations in this potential, to see if the simulation gives results consistent with the theory. We see in Figure 12 that the orbit obtained is circular as expected, the radial oscillations reported are 10^{-8} kpc order of magnitude.

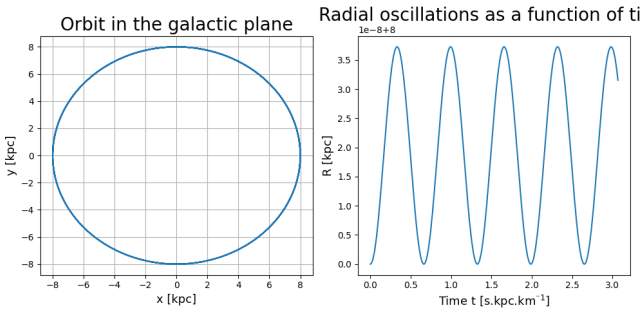

Figure 12: Circular orbit in Plummer potential

B Energy considerations

In order to check the numerical stability of the integration, it is fundamental to check the energy conservation. The total energy of the system is conserved, as is the energy of a particle, given by:

$$E = \frac{v^2}{2} + \Phi(r) \tag{8}$$

Where the velocity can be decomposed such that $v^2 = v_r^2 + v_t^2$, with v_r being the radial velocity and v_t the tangential velocity, which can be written as $v_\theta = r\dot{\theta} = \frac{L}{r}$, with L the angular momentum. In an axis-symmetric distribution where r is the only degree of freedom, the total angular momentum is conserved. In an axis-symmetric potential with two degrees of freedom r, z (3), only the vertical component L_z of the angular momentum is conserved. By substituting into the previous relation, the energy can be written as:

$$\begin{aligned} E &= \frac{v_r^2}{2} + \frac{L^2}{2r^2} + \Phi(r) \\ \iff E &= \frac{\dot{r}^2}{2} + \Phi_{\text{eff}}(r) \end{aligned} \tag{9}$$

Where $\Phi_{\text{eff}}(r) = \frac{L^2}{2r^2} + \Phi(r)$ is the effective potential. In Figure 13, we report the effective potential, as a function of radius, for the case of a Plummer sphere (see (1)), for a value of $L = 455,4\,\text{km}\,\text{kpc}\,\text{s}^{-1}$(left panel) as well as the corresponding temporal oscillation of a particle with this same angular momentum L and energy $E = -2849\,\text{km}^2\,\text{s}^{-2}$(see also blue line in the left panel).

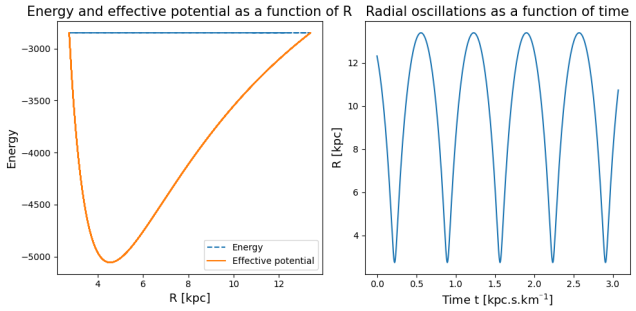

Figure 13: Left panel: Effective potential as a function of radius, for a Plummer distribution and for $L = 455,4\,\text{km}\,\text{kpc}\,\text{s}^{-1}$. Right panel : distance of a particle of angular momentum L and energy $E = -2849\,\text{km}^2\,\text{s}^{-2}$, (see blue line in left panel)

For a given initial energy, provided by the initial position and velocity, we drew an horizontal line on Figure 13, corresponding to the energy of the particle. The particle will oscillate between the intersections of this straight line with the effective potential. For a circular orbit, where the gap between R_{max} and R_{min} tends to 0, the particle will be in the lowest energy state.

References

[1] J. Bovy. "Dynamics and Astrophysics of Galaxies (in preparation)". In: *Princeton University Press* (). URL: https://galaxiesbook.org/index.html.

[2] D. Ceverino et al. "Resonances in barred galaxies". In: *Monthly Notices of the Royal Astronomical Society* 379.3 (Aug. 11, 2007), pp. 1155–1168. ISSN: 0035-8711, 1365-2966. DOI: 10.1111/j.1365-2966.2007.12001.x. URL: https://academic.oup.com/mnras/article-lookup/doi/10.1111/j.1365-2966.2007.12001.x (visited on 12/05/2024).

[3] F. Combes. *Spiral Galaxies*. Version Number: 1. 2023. DOI: 10.48550/ARXIV.2302.12913. URL: https://arxiv.org/abs/2302.12913 (visited on 12/08/2024).

[4] G. Contopoulos et al. "Orbits in weak and strong bars". In: *Astronomy and Astrophysics* 92 (Dec. 1, 1980). ADS Bibcode: 1980A&A....92...33C, pp. 33–46. ISSN: 0004-6361. URL: https://ui.adsabs.harvard.edu/abs/1980A&A....92...33C (visited on 12/08/2024).

[5] S. Ferrone et al. "The e-TidalGCs project: Modeling the extra-tidal features generated by Galactic globular clusters". In: *Astronomy & Astrophysics* 673 (May 2023), A44. ISSN: 0004-6361, 1432-0746. DOI: 10.1051/0004-6361/202244141. URL: https://www.aanda.org/10.1051/0004-6361/202244141 (visited on 12/05/2024).

[6] K. Long et al. "Analytical Potentials for Barred Galaxies". In: *The Astrophysical Journal* 397 (Sept. 1, 1992). Publisher: IOP ADS Bibcode: 1992ApJ...397...44L, p. 44. ISSN: 0004-637X. DOI: 10.1086/171764. URL: https://ui.adsabs.harvard.edu/abs/1992ApJ...397...44L (visited on 12/08/2024).

[7] M. Miyamoto et al. "Three-dimensional models for the distribution of mass in galaxies." In: *Publications of the Astronomical Society of Japan* 27 (Jan. 1, 1975). Publisher: OUP ADS Bibcode: 1975PASJ...27..533M, pp. 533–543. ISSN: 0004-6264. URL: https://ui.adsabs.harvard.edu/abs/1975PASJ...27..533M (visited on 12/05/2024).

[8] H. C. Plummer. "On the Problem of Distribution in Globular Star Clusters: (Plate 8.)" In: *Monthly Notices of the Royal Astronomical Society* 71.5 (Mar. 10, 1911), pp. 460–470. ISSN: 0035-8711, 1365-2966. DOI: 10.1093/mnras/71.5.460. URL: https://academic.oup.com/mnras/article-lookup/doi/10.1093/mnras/71.5.460 (visited on 12/05/2024).

[9] E. Pouliasis et al. "A Milky Way with a massive, centrally concentrated thick disc: new Galactic mass models for orbit computations". In: *Astronomy & Astrophysics* 598 (Feb. 2017), A66. ISSN: 0004-6361, 1432-0746. DOI: 10.1051/0004-6361/201527346. URL: http://www.aanda.org/10.1051/0004-6361/201527346 (visited on 12/05/2024).

[10] E. Vasiliev. "Agama reference documentation". In: (2018). Publisher: arXiv Version Number: 2. DOI: 10.48550/ARXIV.1802.08255. URL: https://arxiv.org/abs/1802.08255 (visited on 12/08/2024).